CHAPTER 4

TRIBOLOGICAL PERFORMANCE OF (Cu-Gr-B_4C) HYBRID COMPOSITES PREPARED BY POWDER METALLURGY ROUTE

4.1 Introduction

The chapter presents the outcomes of fabricating composites using varying weight percentages of B_4C and graphite particles by the powder metallurgy technique. The XRD analysis results for phase identification of pure copper and composites are also shown. The copper composites were analyzed using various techniques to examine the impact of different weight percentages of B_4C and graphite particles on the microstructure, physical and mechanical properties of the composites. The findings and their implications are given and discussed. The dry sliding friction and wear behaviour is observed using the typical pin-on-disc equipment. Both the typical load and the sliding speed have remained unchanged. A counter face composed of EN31 hardened steel is used for the test. The shape, dispersion, and composition of reinforcements have a major impact on the tribological properties of composite materials. The study examines tribological behaviour with respect to several variables, including sliding distance, applied stress, sliding velocity, and the weight percentage of B_4C. The worn surfaces of the composites were examined with a scanning electron microscope (SEM) that was linked to an atomic force microscopy (AFM) and an Energy dispersive x-ray spectroscopy (EDS). The results were related to the topographical analysis of the deteriorated surfaces.

4.2. Copper-based (Cu-Gr-B_4C) hybrid composite

4.2.1 Phase and microstructural analysis

Figure 4.1 illustrates the X-ray diffraction (XRD) pattern of the sintered pure copper, developed composite materials, and neat boron carbide (B_4C) for a diffraction angle of 10° to 90°. The XRD patterns of the sintered composite (CU04) specimen show significant first three peaks at $2\theta \sim 26°$, $2\theta \sim 38°$ and $2\theta \sim 43°$ which are related to the presence of graphite, boron carbide, and copper, respectively. It is also observed that boron carbide and graphite peaks are very

weak in XRD spectra; it is attributed to the low concentration of them in composites. The XRD spectra also show the planes of Cu are (111), (200), and (220), whereas the planes of B_4C and graphite are (104) and (002), respectively. So, the XRD patterns confirm the existence of different phases of materials in the developed sintered composites and pure copper matrix. XRD patterns also reveal that the peaks of B_4C and C in CU04 are more significant than in CU03 and CU02. This is due to the higher concentration of B_4C and graphite in CU04 compared to CU03 and CU02. It is also observed that the peak intensity height increases as reinforcement content increases. The XRD result of composites does not show any peaks of reaction (intermetallic compound) between matrix and reinforcements, so it can be predicted that there is no reaction happening among them. The XRD pattern of hybrid composite specimen CU04 displays the highest peak intensities of reinforcement among all the XRD patterns. This concludes that the reinforcement particles are present in the copper matrix, and higher reinforcement content is responsible for the higher peaks as well. The XRD pattern of the composites did not show any chromium peak; it is attributed to the very low wt.% of it in the composite compared to its matrix wt.%.

The microstructural investigation helps to reveal the presence of reinforcements in the matrix and their distribution, including their bonding with the matrix phases. Figures 4.2 (a) to (d) exhibit the SEM micrographs of the CU01, CU02, CU03, and CU04, respectively. The SEM micrograph of the unreinforced copper (CU01) shows only a similar kind of grain structure, i.e., copper grains, not showing the presence of any foreign element. However, the microstructural examination of developed hybrid composites (CU02, CU03, and CU04) depicts that reinforcements are distributed homogeneously across the matrix, as shown in Figures 4.2 (b) to (d). The homogenous dispersion of reinforcements has a notable impact on the mechanical as well as tribological properties of composites of the materials.

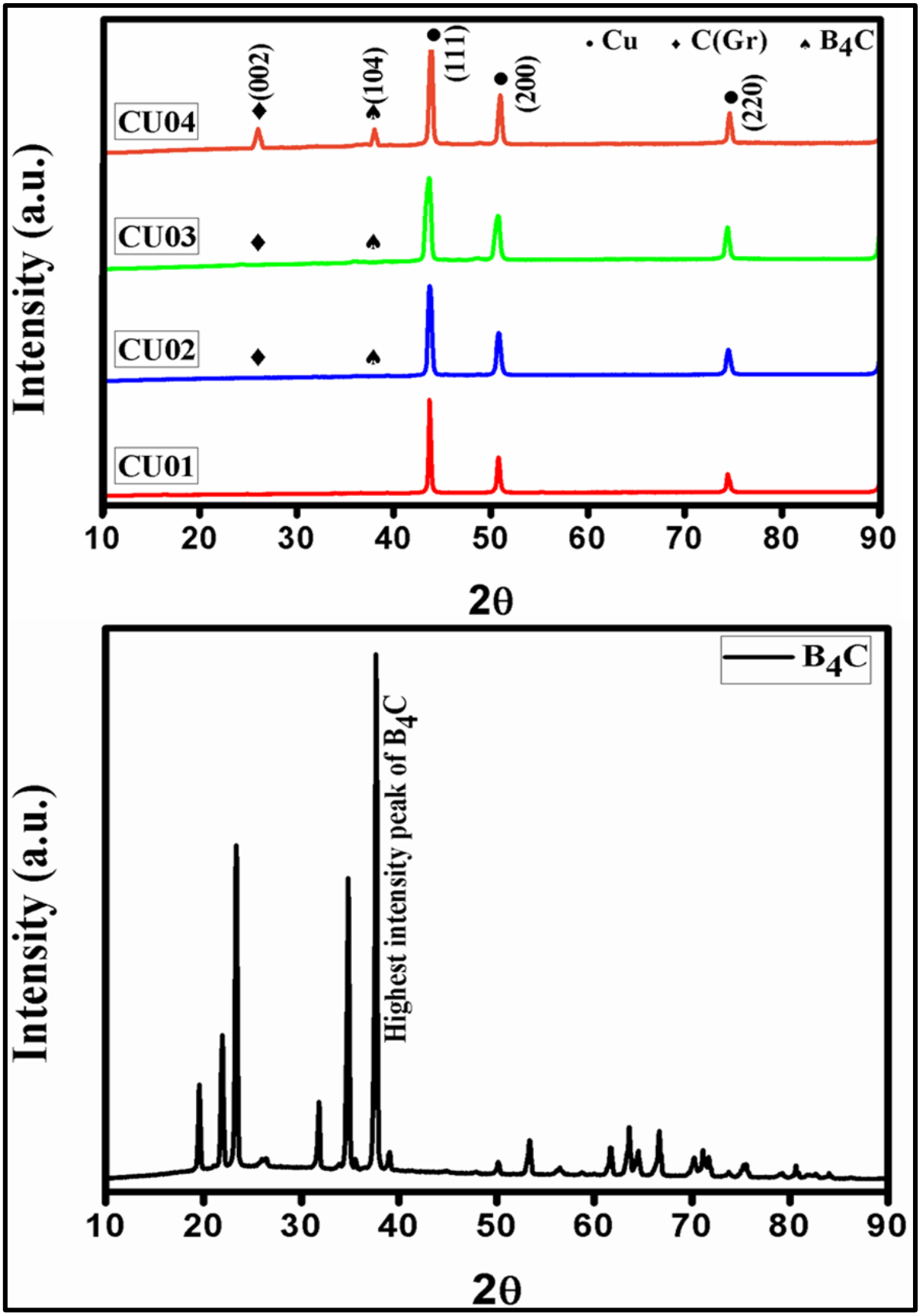

Figure 4.1: XRD spectrum of the developed materials CU01, CU02, CU03, and CU04, including neat B_4C

The SEM micrographs of composites (CU03 and CU04) revealed a higher dispersion of graphite and B_4C particles in the matrix phase as the weight percentage of reinforcement increased, as shown in figures 4.2 (c) and (d). The SEM micrographs also display that there are no cracks developing in the composites with the addition of reinforcement in the copper matrix. Rarely, pores can be observed in the SEM micrographs and also show a rare agglomeration of graphite and B_4C particles at higher content. The lack of micro-cracks in the SEM micrograph of composites suggests that the matrix and particles have sufficient interfacial strength or bonding. However, due to the identical appearance of the B_4C and graphite particles, it is difficult to distinguish them by the naked eye during the microstructural study.

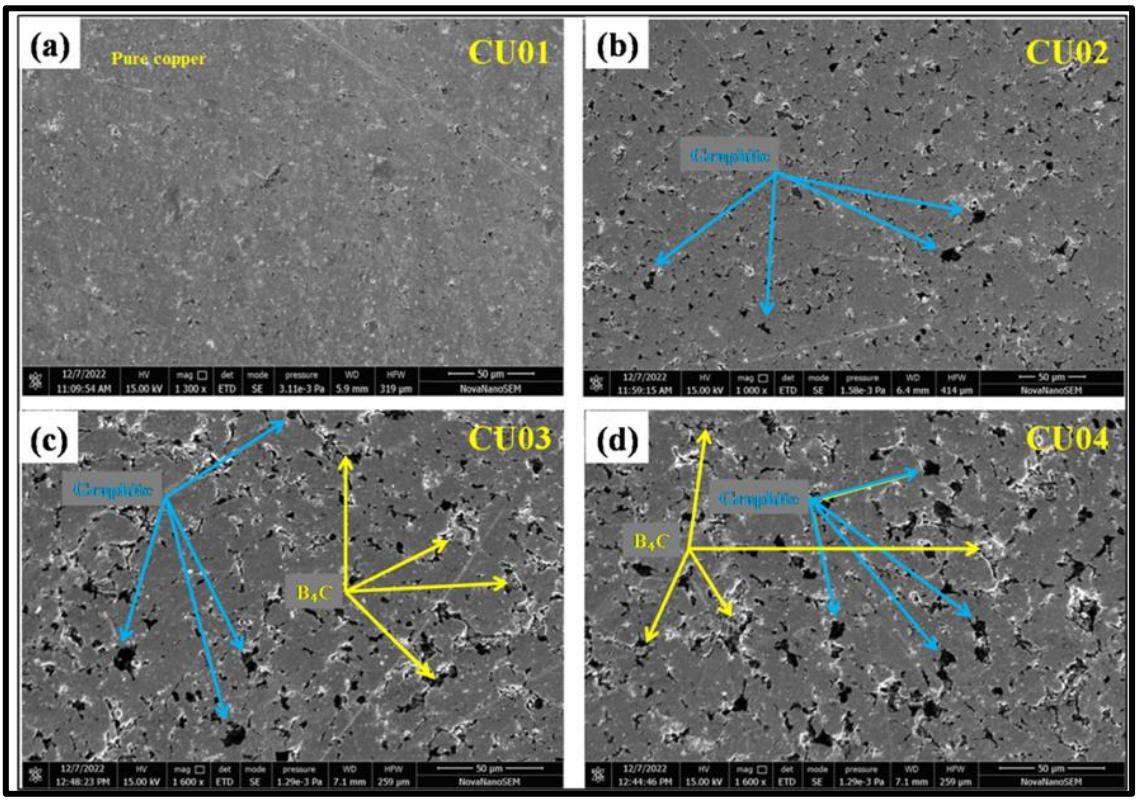

Figure 4.2 SEM micrograph of the developed specimens (a) CU01, (b) CU02, (c) CU03, and (d) CU04.

Therefore, EDS elemental colour mapping is also performed for the developed composite materials to give more strength to the statement about the presence of reinforcing materials in

the matrix for the SEM images, as shown in Figure 4.2. The EDS element colour mapping analysis of developed composites (CU02) and (CU04) specimens with their concentration tables is shown in Figure 4.3. The elemental color mapping micrograph and concentration table of composites shows the presence of every element, i.e., copper (Cu), chromium (Cr), boron(B), and carbon(C), as shown in Figure 4.3. Graphite represents a crystalline structure of carbon embedded within the matrix. Distinguishing boron carbide from graphite in carbon form through elemental colour mapping presents significant challenges, as both materials contain carbon elements.

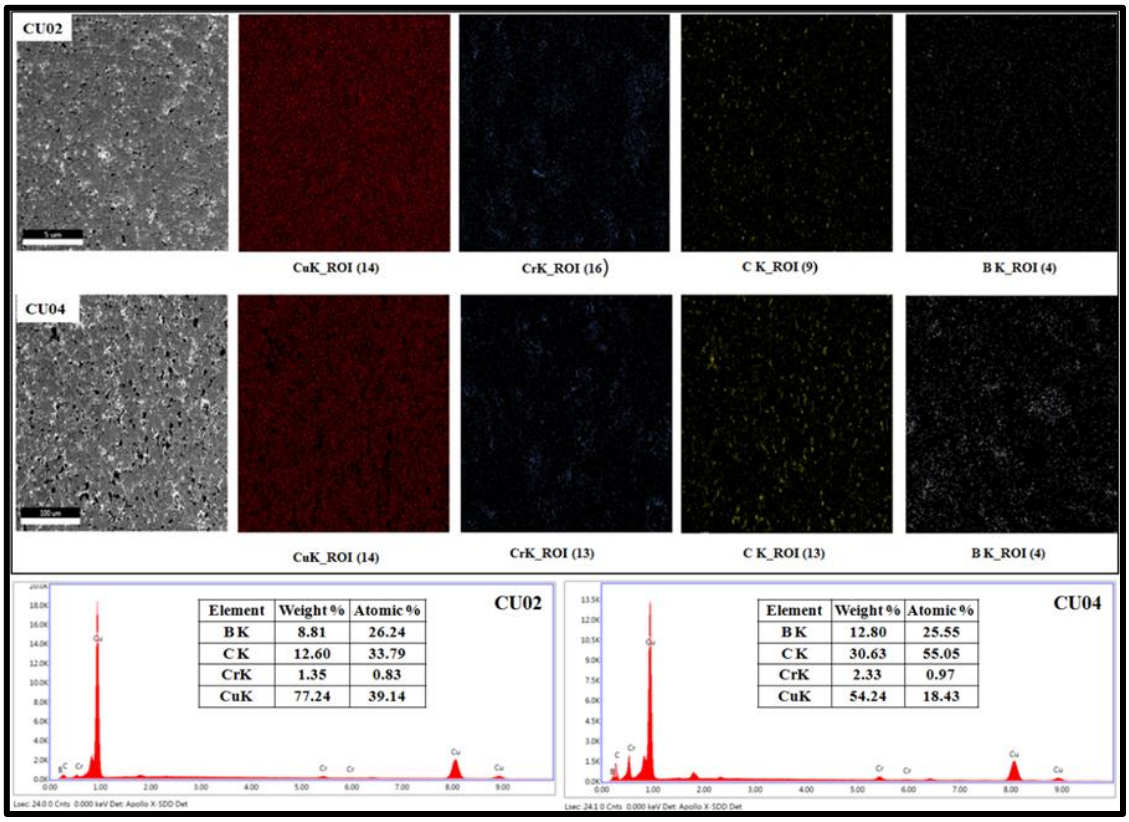

Figure 4.3. Energy dispersive x-ray spectroscopy (EDS) Elemental color mapping of CU02 and CU04 composite specimens with their concentration tables.

4.2.2 Physical and mechanical properties

Table 4.1 shows the details of the theoretical density, sintered (experimental) density, porosity, and hardness of the developed materials. From the table, it is very clear that the sintered or experimental densities and theoretical densities of composite specimens are lower than the unreinforced copper specimens. It is attributed to the reinforcement of lighter materials such as graphite (2.20 g/cm3) and boron carbide(B_4C) (2.52 g/cm3) in the copper matrix (Samal et al.,

2013). It is also observed that the experimental density and theoretical density of the composites decrease as reinforcement particles increase in the matrix. On addition of graphite and boron carbide (B_4C) with a total weight of 3 wt.% in the matrix, the sintered or experimental density of composites falls from 8.49 g/cm3 to 7.46 g/cm3, as shown in the table, and it decreases on further addition of reinforcement in the copper matrix. The composite (CU04) shows the least experimental and theoretical density among all developed materials. The material's density is also influenced by various variables, including the particle's size, nature, shape, and composition of the material (Jamwal et al., 2020). From table 4.1, higher porosity is observed in composites compared to their matrix and it increases when the weight percentage of graphite and boron carbide increases. It is attributed to the uniform distribution of graphite and boron carbide particles, albeit with a proclivity for agglomerates to form at selected matrix sites, which leads to an increase in porosity.

Table 4.1 illustrates the Vickers hardness variation of all the developed materials. The test results indicate that the composites' hardness improved significantly with the addition of graphite and B_4C to the copper metal matrix. It is observed that the hardness of developed materials increases with increasing weight percentage of reinforcement, it reaches a hardness value of 87.4 ± 1 from 58 ± 1.5 on reinforcement addition of total 3 wt.% and 98.7 ± 2.2 from 58 ± 1.5 on reinforcement addition of total 6 wt.% in copper matrix. It is a 69% improvement in the hardness value of CU03 over pure copper matrix. However, on further addition of a reinforcement total of 9 wt.% in the copper matrix the hardness value decreases to 82.5 ± 0.5 as compared to other composites but is still higher than its matrix. The improvement in hardness of the developed composites is due to the addition of B_4C, which is harder in nature (third hardest available material) as compared to the copper matrix (Singh & Gautam, 2019). It is also attributed to the B_4C ceramic particle in the copper matrix; it has a very good interfacial bonding with the copper matrix, and the B_4C particle's ability to prevent dislocation motion

also exists (Alizadeh et al., 2015; Baradeswaran et al., 2014; Çelik & Seçilmiş, 2017). However, the lowering of hardness value in the composite with a total of 9 wt.% reinforcement in the matrix is attributed to the soft nature of graphite and its quite high porosity(Miranda-López et al., 2021).

Table 4.1 Theoretical density, sintered (experimental) density, porosity, and hardness of the developed materials.

S. No.	Developed materials	Theoretical density (g/cm^3)	Sintered/experimental density (g/cm^3)	Porosity (%)	Hardness (Hv)
1	CU01	8.96	8.49 ± 0.13	5.25 ± 0.11	58.3 ± 1.5
2	CU02	8.22	7.46 ± 0.12	9.25 ± 0.13	87.4 ± 1
3	CU03	7.63	6.72 ± 0.14	11.93 ± 0.11	98.7 ± 2.2
4	CU04	7.12	6.14 ± 0.11	13.76 ± 0.12	82.5 ± 0.5

4.2.3 Dry sliding friction and wear

4.2.3.1 Effect of sliding distance

Figure 4.4 exhibits the behaviour of the friction coefficient with the sliding distance for the developed CU01, CU02, CU03, and CU04 materials. The nature of the friction coefficient with sliding distance is fluctuating. However, from the Figure, it is observed that the friction coefficient of the developed composites (CU02, CU03, and CU04) is quite lower as compared to the friction coefficient of CU01. Since, from the Figure, it is quite difficult to say the exact value of the friction coefficient, the average value is reported in the further results.

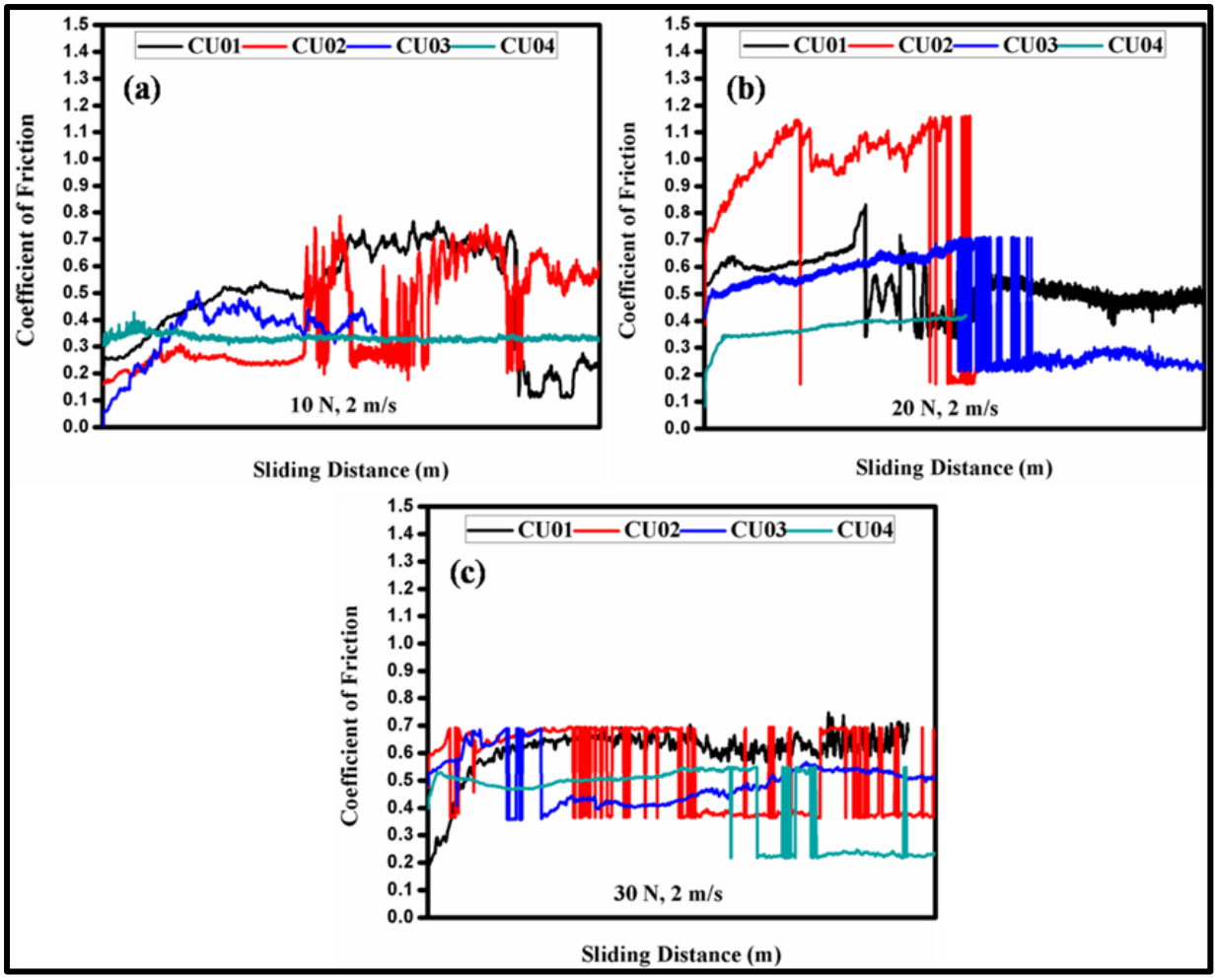

Figure 4.4. The variation of the friction coefficient with the sliding distance for CU01, CU02, CU03, and CU04

4.2.3.2 Effect of Boron Carbide(B_4C) and Graphite (Gr) Content

Figure 4.5(a) illustrates the variation in wear rate of developed composite materials with reinforcement concentrations at normal loads of 10, 20, and 30 N and a sliding speed of 2 m/s for a sliding distance of 2 km. From the Figure, it is observed that as the reinforcement content increases, the wear rate decreases in all the developed materials at all the applied loads of 10, 20, and 30 N. However, the wear rate increases with an increase in the applied normal load for all the developed materials. The wear rate of CU04 is 16%, 42%, and 61% lower than the wear rates of CU03, CU02, and CU01, respectively, i.e., CU04 exhibits the lowest wear rate among all the developed materials at 10, 20, and 30 N applied loads and a sliding speed of 2 m/s for a

sliding distance of 2 km. Such improvement in wear resistance of developed composites is attributed to the addition of a higher wt.% of graphite, which acts as a solid lubricant to a greater extent during the surface interaction of the wear pin and counter disc (Rajkumar and Aravindan, 2011). The wear resistance of developed composites is also improved due to the presence of extremely hard B_4C particles and also shows very good interfacial bonding in the copper matrix, which prevents plastic deformation of composites, i.e., the composite materials become harder with the addition of harder B_4C particles (Siddesh Kumar et al., 2020). Figure 4.5 (b) shows the variation of the COF with different weight percentages of reinforcement in copper matrix at 10, 20, and 30 N applied to normal loads and a sliding speed of 2 m/s for a sliding distance of 2 km. From Figure 4.5 (b), it is observed that the COF values decrease as the content of reinforcement increases for all the applied normal loads and sliding speed of 2 m/s. It is seen that the COF for the CU01, CU02, CU03, and CU04 specimens is 0.607, 0.563, 0.501, and 0.424, respectively, at a maximum applied normal load of 30 N. The COF of specimen CU04 is approx 30%, 24%, and 15% lower as compared to that of specimens CU01, CU02, and CU03, respectively, at the applied normal load of 30 N. Such a trend in COF of developed composites is due to the reinforcement of graphite in the matrix, which has a good lubricating property. The graphite particles from the composites will be exposed soon when they interact with the counter-rotating disc, which creates a lubricating surface in between the mating surfaces, so further mating of surfaces will diminish. The phenomenon is conceivable because graphite has good solid lubricant properties. This reduction of COF in developed composite materials may also be due to the reinforcement of harder B_4C which may develop point contact with the counter disc and form some boron oxide layer, which is a key parameter in reducing the COF (Çelik and Seçilmiş, 2017). The statement is supported by some literature reports a similar outcome in cases where hard titanium carbide and graphite particles coexist within a soft matrix (Rajkumar and Aravindan, 2011; Kumar et al., 2023).

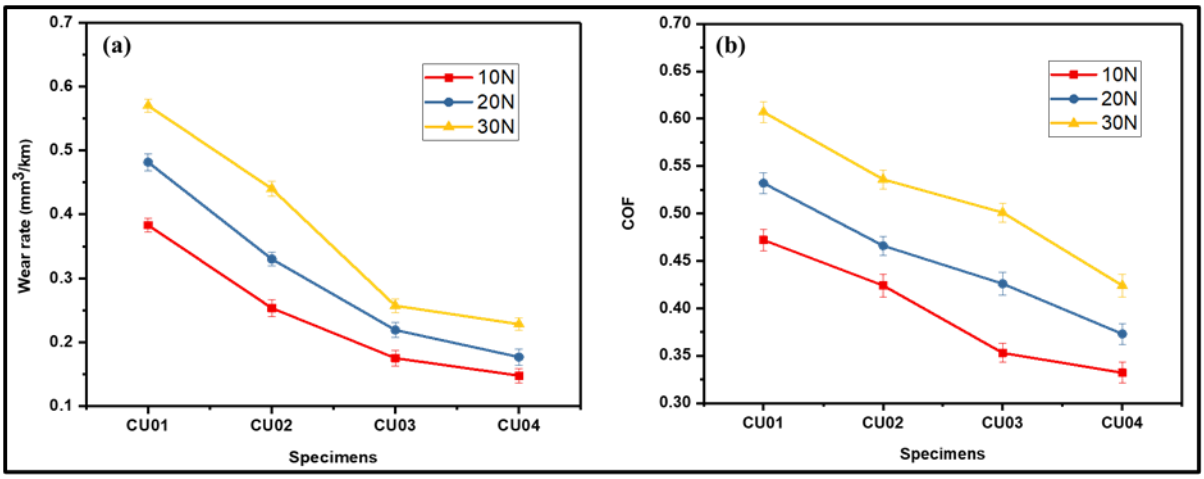

Figure 4.5. Influence of reinforcement on (a) wear rate and (b) COF at applied normal loads of 10, 20, and 30 N and sliding velocity of 2 m/s for a sliding distance of 2 km

4.2.3.3 Effect of applied normal load

Figure 4.6(a) illustrates the behaviour of the wear rate of CU01 and CU02, CU03, and CU04 specimens at different applied normal loads of 10, 20, and 30 N at 2 m/s sliding speed for a sliding distance of 2 km under dry sliding conditions. It is observed that the average wear rate of CU01, CU02, CU03, and CU04 increases with an increase in applied normal loads at a sliding speed of 2 m/s. The CU01 shows the highest wear rate among all the developed materials at all the applied normal loads and increases as the load increases, too. During the dry sliding of CU01, a thin oxide layer will develop after some testing and cover its surfaces. This developed oxide film is at a lower load, which is not enough to break such an oxide layer, so it prevents the CU01 surface from coming into direct contact with the rotating counter disc surface. Therefore, the wear rate at a lower applied normal load shows a lower value, and in this process, the wear is mildly oxidative. However, at higher applied normal loads, such developed oxide layer will start damaging soon, which will expose the new surface of CU01, and this will be a continuous process at higher loads, which leads to a higher wear rate. In addition to this, at higher applied normal load, the contacting temperature will also be high, which leads to more oxidation and the development of oxide layers that are brittle in nature

and damage easily at higher applied loads. However, the reduction in wear rate of developed composites is observed as the weight fraction of B_4C and graphite increases due to the wear resistance developed by the combined effect of B_4C and graphite reinforcements in the matrix. Although, the wear rate of developed composite materials increases as the applied normal load increases, it may be attributed to the breaking of oxidative layers and the pulling out of hard ceramic from the pin surface, which stuck between the mating surfaces and starts acting as a third body abrasion between the surfaces (Siddesh Kumar et al., 2020; Berman et al., 2015). Figure 4.6(b) displays the variation of COF with applied normal loads for developed materials CU01, CU02, CU03, and CU04 at 2 m/s sliding speed for a sliding distance of 2 km under dry sliding conditions. From the Figure, it has been noticed that as the applied normal load increases, the COF increases for all the developed materials. The developed material CU01 exhibits the highest COF among all the applied normal load conditions. This is attributed to the adhesive characteristics of tribo-contact, which leads to the movement of the soft copper matrix towards the harder countertop surface, and higher plastic deformation occurs as the applied load increases, which raises the COF value.

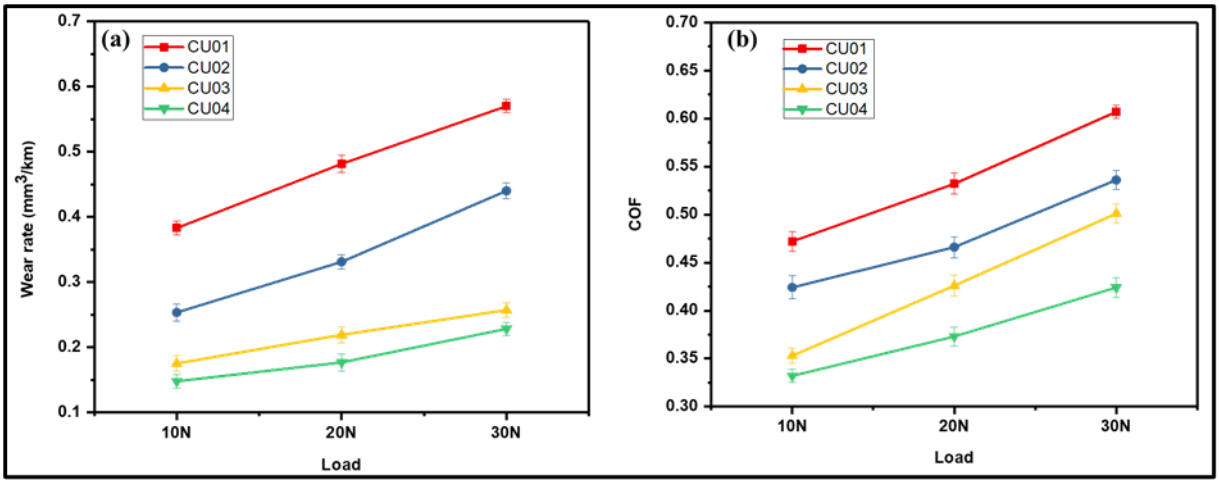

Figure 4.6 Effect of applied normal loads on (a) wear rate and (b) COF at a sliding velocity of 2 m/s for a sliding distance of 2 km

However, in the developed composites, the harder B_4C particles may come out of the pin surface at higher applied normal loads and contribute to an increase in the COF value.

4.2.3.4 Effect of Sliding Speed

Figure 4.7(a) displays the effect of sliding speed on the wear rate of the developed materials CU01, CU02, CU03, and CU04 at an applied normal load of 30 N for a sliding distance of 2 km. From the Figure, it is observed that the wear rate of all developed materials increases as the sliding speed increases from 1 m/s to 2 m/s for the same applied normal load and sliding distance. It is also depicted that the CU01 has the highest wear rate among all the developed materials at both sliding speeds of 1 and 2 m/s. Whereas the developed composites show a decreasing wear rate as the content of reinforcement increases for both sliding speeds of 1 and 2 m/s. However, the wear rate of the developed hybrid composites is higher at a sliding speed of 2 m/s as compared to the wear at 1 m/s at an applied normal load of 30 N and a sliding distance of 2 km. So, it can be concluded that the wear rate of all the developed materials is slightly influenced by changes in sliding speed under dry sliding conditions. The wear rate for the CU01 specimen is 35% higher at a sliding speed of 2 m/s as compared to the wear rate of theCU01 at a sliding speed of 1 m/s at applied normal load of 30 N. However, the percentage rise in wear rate with the increase in sliding speed from 1 to 2 m/s is 32%, 16%, and 14%, in the CU02, CU03, and CU04 composites, respectively, for the applied normal load of 30 N. Such behaviour of an increase in wear rate of developed composites with an increase in sliding speed is attributed to the more reinforcing particles to be pulled out of the composites, including the strained hardened copper particle. This Pulled out hard particles and work hardened particles are certainly trapped between the contacting surfaces, these hard particles act as a third body between the two mating surfaces, increasing the wear rate due to the third body abrasion as well (Ankit et al., 2023).

Figure 4.7(b) illustrates the effect of sliding speed on COF of developed materials CU01, CU02, CU03, and CU04 at an applied normal load of 30 N for a sliding distance of 2 km. From the Figure, it has been observed that the COF of developed materials increases as the sliding speed increases from 1 m/s to 2 m/s at an applied normal load of 30 N for a sliding distance of 2 km under dry sliding conditions. The COF for the specimens CU01, CU02, CU03, and CU04 increased by 6.12%, 11.23%, 10%, and 4%, respectively, when the sliding speed increased from 1 m/s to 2 m/s at a normal load of 30 N. This increment of COF in CU01 with the increment of sliding speed specimen may be attributed to the development of a harder oxide layer due to increases in temperature at mating surfaces. This hard surface will reduce the area of mating surfaces, i.e., point contact. However, in developed composite materials, the hard ceramic particles of B_4C may mechanically comminute with the graphite particles between the mating surfaces and the adherent film generated, which leads to an increase in COF.

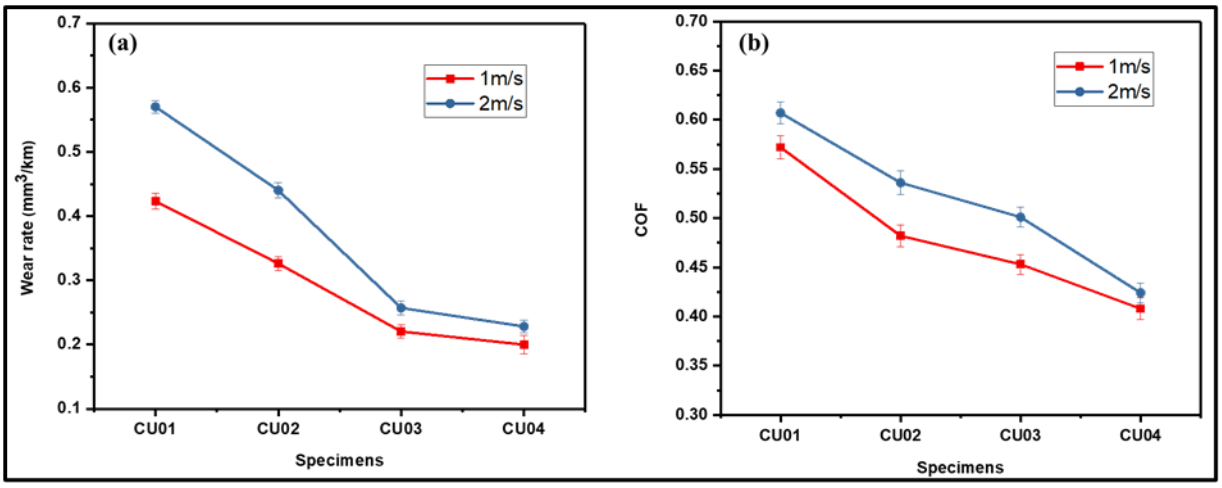

Figure 4.7. Effect of sliding speeds on (a) wear rate and (b) COF of developed materials at an applied normal load of 30 N for a sliding distance of 2 km

4.2.4 Analysis of Surfaces before and after deteriorated

4.2.4 1. The deteriorated surface at a normal load of 30 N for all specimen

Figures 4.8 (a) and 4.8 (b) display the SEM micrographs of the worn surface of the CU01 at an applied normal load of 30 N for a sliding distance of 2 km at sliding speeds of 1 m/s and 2 m/s,

respectively. However, Figures 4.8 (c) and (d) exhibit the SEM micrographs of the worn surface of the CU02 at an applied normal load of 30 N for a sliding distance of 2 km at sliding speeds of 1 m/s and 2 m/s, respectively. The worn surface of the CU01 specimen exhibits a consistent, narrow groove at a sliding speed of 1 m/s and an applied normal load of 30 N, as shown in Figure 4.8 (a). Figure 4.8 (b) reveals the extensive delamination at a high sliding speed of 2 m/s at 30 N applied to a normal load. Such a wear phenomenon happened with CU01 at both sliding speeds of 1 and 2 m/s, attributed to the hardened EN 30 counter steel disc's asperity, which caused significant abrasion and deep cuts to the pure copper's surface. Therefore, the COF and wear rate of pure copper specimens are higher as compared to their composites, as reported above. At a higher sliding speed of 2 m/s, there is considerable adhesion between the contacting surfaces, resulting in significant delamination from the softer copper matrix, as shown in Figure 4.7 (b). However, the micrographs of the worn surfaces of hybrid composite (CU02) show very few groves and delamination as compared to pure copper at an applied normal load of 30 N for sliding speeds of 1 and 2 m/s, as shown in Figures 4.8 (c) and 4.8 (d), respectively. This is attributed to the lubricating behaviour of graphite reinforcement, which leads to smoother worn surfaces. In addition, the reinforcement of B_4C the copper matrix has increased the hardness, which definitely improves the wear resistance during dry sliding also (Anil et al., 2017; Berman et al., 2013).

the wear behavior of pure copper, the primary mode of wear is attributed to adhesion, leading to delamination. The strong adhesive forces between the ductile matrix and the mating surface result in material transfer and subsequent delamination. In the case of graphite (Gr) reinforcement, we observed a notable deviation from the delamination mechanism. Graphite acts as a lubricating layer during wear, significantly reducing adhesion and preventing delamination. This effect can be attributed to the self-lubricating properties of graphite, which create a protective layer between the mating surfaces, thereby altering the wear mechanism.

For B_4C reinforcement, Initially, copper undergoes abrasion due to wear between the copper matrix and the metallic counter surface. Subsequently, when fresh boron carbide (B_4C) hard particles are exposed, they act as wear resistance agents. Additionally, the formation of B_2O_3 oxide occurs, serving as a protective layer, which effectively reduces wear. This dual action of B_4C as both a hard particle for abrasion and a contributor to the formation of a protective layer is a crucial aspect of the composite's tribological performance. Therefore, Increased B_4C and graphite content in the composites causes the wear mechanism to change from delamination to a combination of abrasive, oxidative, and delamination wear.

Figures 4.8 (e) and 4.8 (f) display the SEM micrographs of the worn surface of the CU03 at an applied normal load of 30 N for a sliding distance of 2 km at sliding speeds of 1 m/s and 2 m/s, respectively. However, Figures 4.8 (g) and 4.8 (h) exhibit the SEM micrographs of the worn surface of the CU04 at an applied normal load of 30 N for a sliding distance of 2 km at sliding speeds of 1 m/s and 2 m/s, respectively. Figure 4.8 (e) displays the delamination and cracks on the worn surface of the CU03 specimen at low sliding velocity (1 m/s), while Figure 4.8 (f) depicts the wide ploughing marks on the worn surface at high sliding velocity (2 m/s). However, the worn surface in the hybrid composite specimen of CU04 exhibited more changes in appearance as B_4C and graphite particle contents were raised, as shown in Figures 4.8 (g) and 4.8 (h). Figure 4.8 (g) exhibits the smooth plough marks in the direction of sliding on the worn surface of CU04. It also displays the signs of smooth ploughing, including fine cracks, larger-sized wear debris, and oxide layer deposition. It concludes that the mechanism of wear changes from delamination to the combination of delamination and abrasion as the amount of B_4C and graphite reinforcement increases in the composite. It is also observed that the development of wear debris at a high speed leads to cracking. The higher B_4C and graphite concentrations in the copper matrix have enhanced its hardness, which can significantly increase its wear resistance by preventing the matrix from deforming while sliding against the

counter surface (Kanagaraj et al., 2010; Kumar et al., 2017; Song et al., 2020). Because of graphite's solid lubricant nature, raising the reinforcement wt.% improves composite material wear resistance. However, the softness of graphite affects the hardness of composite materials. During mechanical characterization, sites with uniformly distributed graphite are weak and deform easily. However, to compensate for this hardness loss, we must reinforce hard ceramic material (B_4C), which increases the hardness of composite material. To balance the mechanical and tribological properties of the produced composite material, we used an equal wt.% of reinforcement. According to Archard's wear law, wear resistance is determined by both the material's hardness and its solid lubricant properties. Graphite predominates over boron carbide in the CU04 specimen.

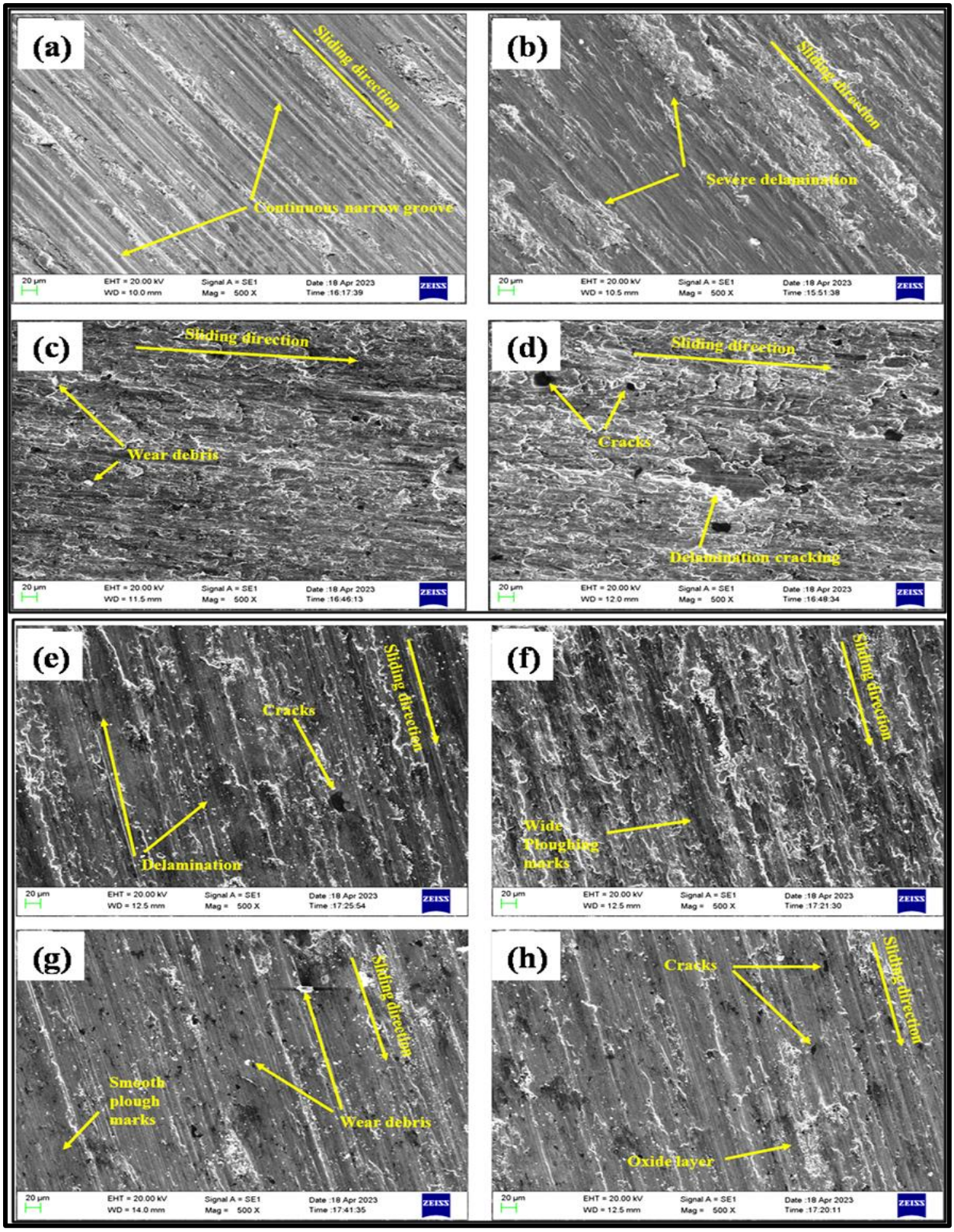

Figure 4.8 SEM micrograph of the worn surface at 30 N load for a sliding distance of 2 km of (a) CU01, (c) CU02, (e) CU03, and (g) CU04 at a sliding speed of 1 m/s and (b) CU01, (d) CU02, (f) CU03, and (h) CU04 at a sliding speed of 2 m/s.

4.2.4.2 Energy dispersive x-ray spectroscopy (EDS) elemental color mapping and spectrum of the deteriorated surface at 30 N load

The EDS elemental colour mapping study is performed to better analyse the worn surfaces of the developed composite and reveal its wear mechanism during the tribo-test. Figures 4.9 (a) and 4.9 (b) depict the worn surfaces of CU02 and their respective EDS elemental colour mapping at an applied normal load of 30 N for a sliding distance of 2 km at sliding speeds of 1 m/s and 2 m/s, respectively. From Figures 4.9 (a) and 4.9 (b), the EDS elemental color mapping of various elements such as copper (Cu), chromium (Cr), carbon(C), boron(B), oxygen(O), and Fe is observed on the worn surface of CU02 at both the sliding speeds of 1 m/s and 2 m/s. So, it can be concluded that the oxidative, abrasive, and adhesive wear mechanisms are involved during the dry sliding tribo-test of the developed composite CU02. The presence of Cu, Cr, C, and B elements in the colour mapping is easy to understand because it is involved in the development of composites. But the presence of the O element may be attributed to the formation of oxides due to the rise in temperature of the interacting surfaces at the higher applied normal load of 30 N during the dry sliding tribo-test. However, the presence of Fe may be attributed to the wearing of counter steel discs in a lesser amount at a higher applied load of 30 N during the dry sliding wear test. Figure 4.9 (b) reveals that the dot concentration in the elemental colour mapping of C is higher at a sliding speed of 2 m/s as compared with the same at a sliding speed of 1 m/s. It may be attributed to the early exposure of graphite particles at a higher sliding speed of 2 m/s and a normal applied load of 30 N. However, it is observed that the dot concentration in the elemental colour mapping of Fe at a sliding speed of 2 m/s is lower as compared with the same at a sliding speed of 1 m/s. It may be attributed to a reduction in the proper contact of the interacting surfaces at higher sliding speed of 2 m/s. To support the above statement regarding the EDS colour mapping of the CU02 worn surface at different sliding speeds of 1 m/s and 2 m/s, its peak spectrum and concentration table are also shown in Figures 4.10 (a) and 4.10 (b), respectively.

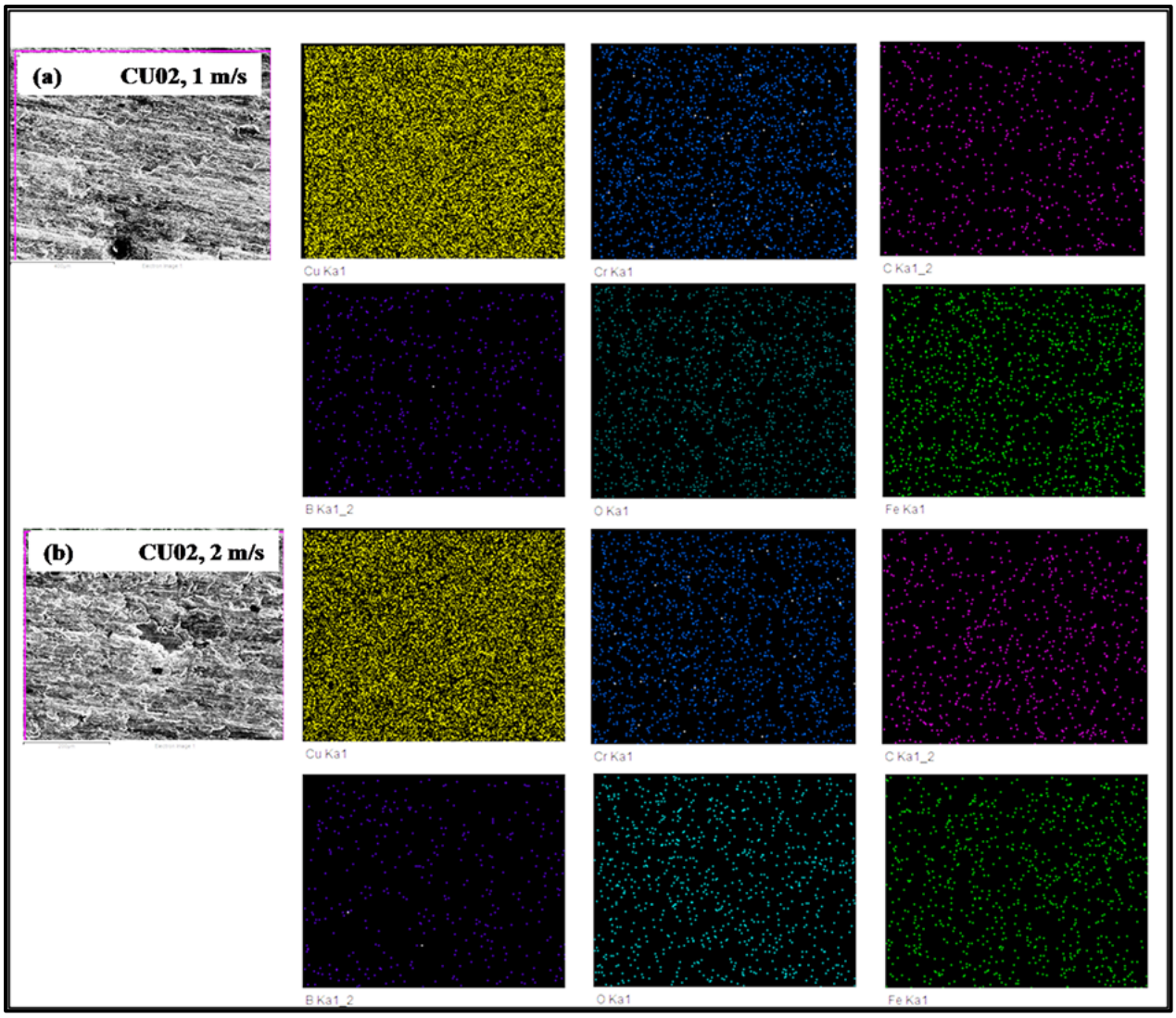

Figure 4.9 Energy dispersive x-ray spectroscopy (EDS) elemental colour mapping of the worn surface of CU02 at an applied normal load of 30 N for a sliding distance of 2 km

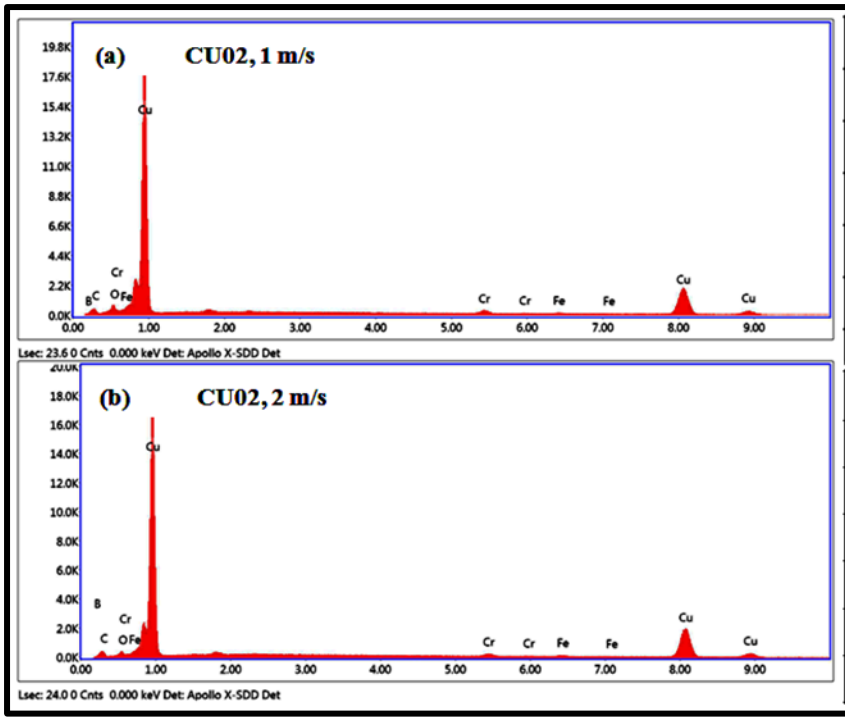

Element	Weight %	Atomic %
BK	10.62	29.02
CK	12.35	30.37
OK	3.25	6.00
CrK	2.38	1.35
FeK	1.32	0.70
CuK	70.07	32.57

Element	Weight %	Atomic %
BK	8.58	25.29
CK	12.18	32.29
OK	1.68	3.34
CrK	1.32	0.81
FeK	0.61	0.35
CuK	75.63	37.92

Figure 4.10 Energy dispersive x-ray spectroscopy (EDS) spectrum and element concentration table of the worn surface of CU02 at sliding speeds of (a) 1 m/s and (b) 2 m/s

Figures 4.11 (a) and 4.11 (b) exhibit the worn surfaces of CU04 and its corresponding EDS elemental colour mapping at an applied normal load of 30 N for a sliding distance of 2 km at a sliding speed of 1 m/s, and 2 m/s, respectively. Figures 4.11(a) and 4.11(b) also display the presence of elements such as: copper (Cu), chromium (Cr), carbon(C), boron(B), oxygen(O), and Fe in the EDS elemental colour mapping of the worn surfaces of the CU04 specimen at both the sliding of 1 m/s and 2 m/s. The reason for including these elements in the mapping is the same as discussed above for Figure 4.9. In Figure 4.11, the density of the carbon dots is almost the same in the colour mapping of the worn surface of CU04 at both sliding speeds, which suggests the stable state of the graphite layer developed in CU04 as compared to the unstable graphitic state observed in the CU02 specimen during the mapping analysis, as shown in Figure 11. After the analysis of the colour mapping of the worn surface of CU04, it can be stated that the oxidative, abrasive, and adhesive wear mechanisms are also involved in CU04.

To support the above statement regarding the EDS colour mapping of the CU04 worn surface at different sliding speeds of 1 m/s and 2 m/s, its peak spectrum and concentration table are also shown in Figures 4.12 (a) and 4.12 (b), respectively.

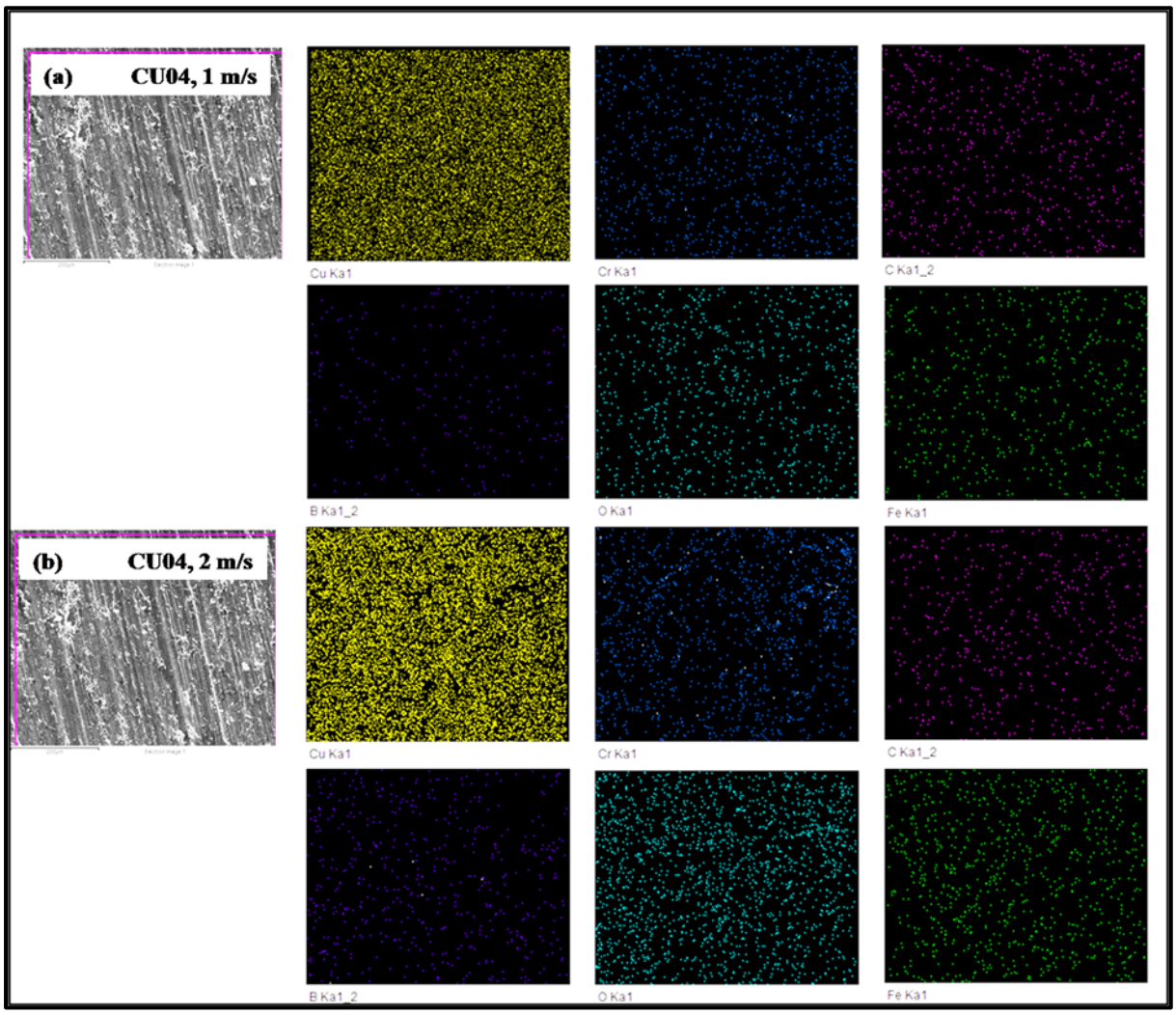

Figure 4.11 Energy dispersive x-ray spectroscopy (EDS) elemental colour mapping of the worn surface of CU04 at an applied normal load of 30 N for a sliding distance of 2 km

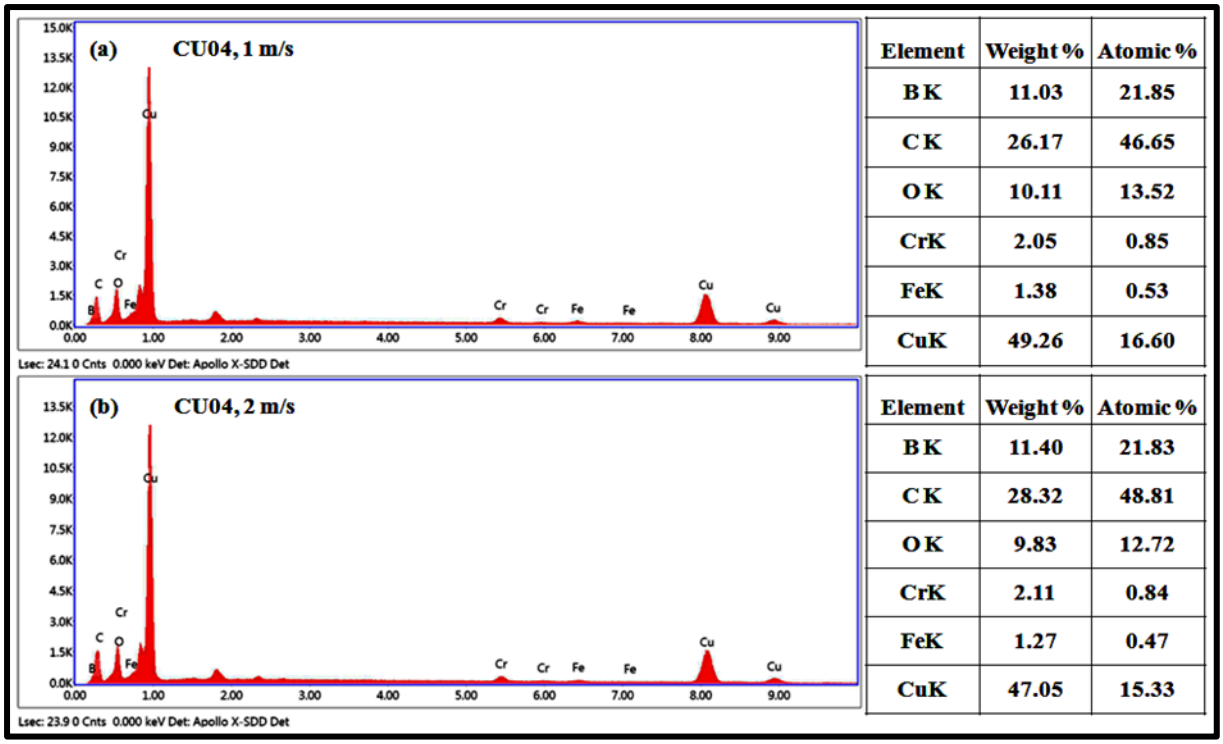

Element	Weight %	Atomic %
B K	11.03	21.85
C K	26.17	46.65
O K	10.11	13.52
CrK	2.05	0.85
FeK	1.38	0.53
CuK	49.26	16.60

Element	Weight %	Atomic %
B K	11.40	21.83
C K	28.32	48.81
O K	9.83	12.72
CrK	2.11	0.84
FeK	1.27	0.47
CuK	47.05	15.33

Figure 4.12 Energy dispersive x-ray spectroscopy (EDS) spectrum and element concentration table of the worn surface of CU04 at sliding speeds of (a) 1 m/s and (b) 2 m/s

Figures 4.13(a), 4.13(b), 4.13(c), and 4.13(d) display the SEM, EDS, and elemental concentration table of the developed material's samples before friction tests CU01, CU02, CU03, and CU04, respectively. From Figure 4.13, it can be observed that the weight percentage of boron and carbide increases as the reinforcement weight percentages increase in the copper matrix. The Figures do not show any kind of wear track on them as well.

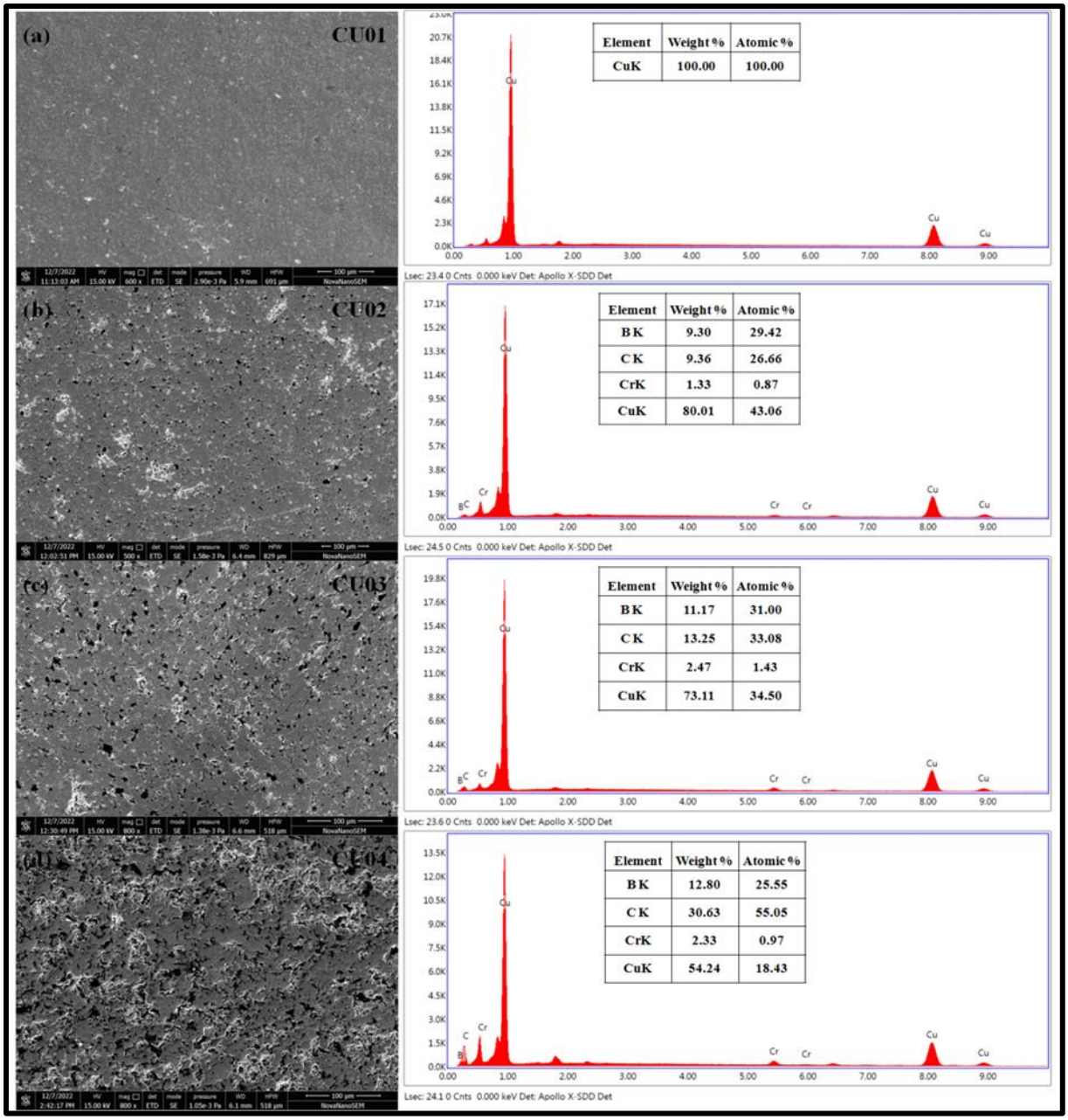

Figure 4.13 SEM, Energy dispersive x-ray spectroscopy (EDS), and elemental concentration table of the samples before friction tests, (a) CU01, (b) CU02, (c) CU03, and (d) CU04

4.2.5 Atomic force microscopy (AFM)analysis of deteriorated surfaces

Figures 4.14(a), 4.14(c), and 4.14(e) depict the atomic force microscopy (AFM) 3D images of worn surfaces of the developed materials CU01, CU02, and CU04, respectively, at a sliding speed of 1 m/s and an applied normal load of 30 N for a sliding distance of 2 km. However, Figures 4.14(b), 4.14(d), and 4.14(f) display the atomic force microscopy (AFM) 3D images

of worn surfaces of the developed materials CU01, CU02, and CU04, respectively, at a sliding speed of 2 m/s and an applied normal load of 30 N for a sliding distance of 2 km. The scanning probe microscopic examination is very well suited to analysing the surface roughness and micro-texture of the worn surfaces of the developed materials. For the AFM analysis, 50 μm of the worn surface of the developed materials is considered. Figures 4.14(a) and 4.14(b) exhibit very clearly that the peaks value of the worn surface of CU01 at a sliding speed of 2 m/s is higher than the peaks value of the worn surface of CU01 at a sliding speed of 1 m/s, which suggests that the wearing of materials is high at a higher sliding speed. A similar pattern is also observed in the peak value of worn surfaces of CU02, as shown in 4.14(c) and 4.14(d). However, it seems the same level of peak value of the worn surface of CU04 is observed in its SPM micrograph at sliding speeds of 1 m/s and 2 m/s, as shown in Figures 4.14(e) and 4.14(f), although wear loss is higher at sliding speeds of 2 m/s as compared to loss at sliding speeds of 1 m/s as reported above. From Figure 4.14, it is also observed that the peak value intensity of composite worn surfaces is lower as compared to the peak value intensity of copper matrix at both sliding speeds of 1 m/s and 2 m/s; it concludes that the wear loss in composites is lower as compared to mean square roughness (Rq), as shown in Table 4.2. The CU04 specimen has shown the least surface roughness (Ra) at both the sliding speeds of 1 m/s and 2 m/s, which supports the statement above that, the CU04 specimen has the least amount of wear loss. These AFM test results align with the SEM findings at various sliding speeds reported above their matrix.

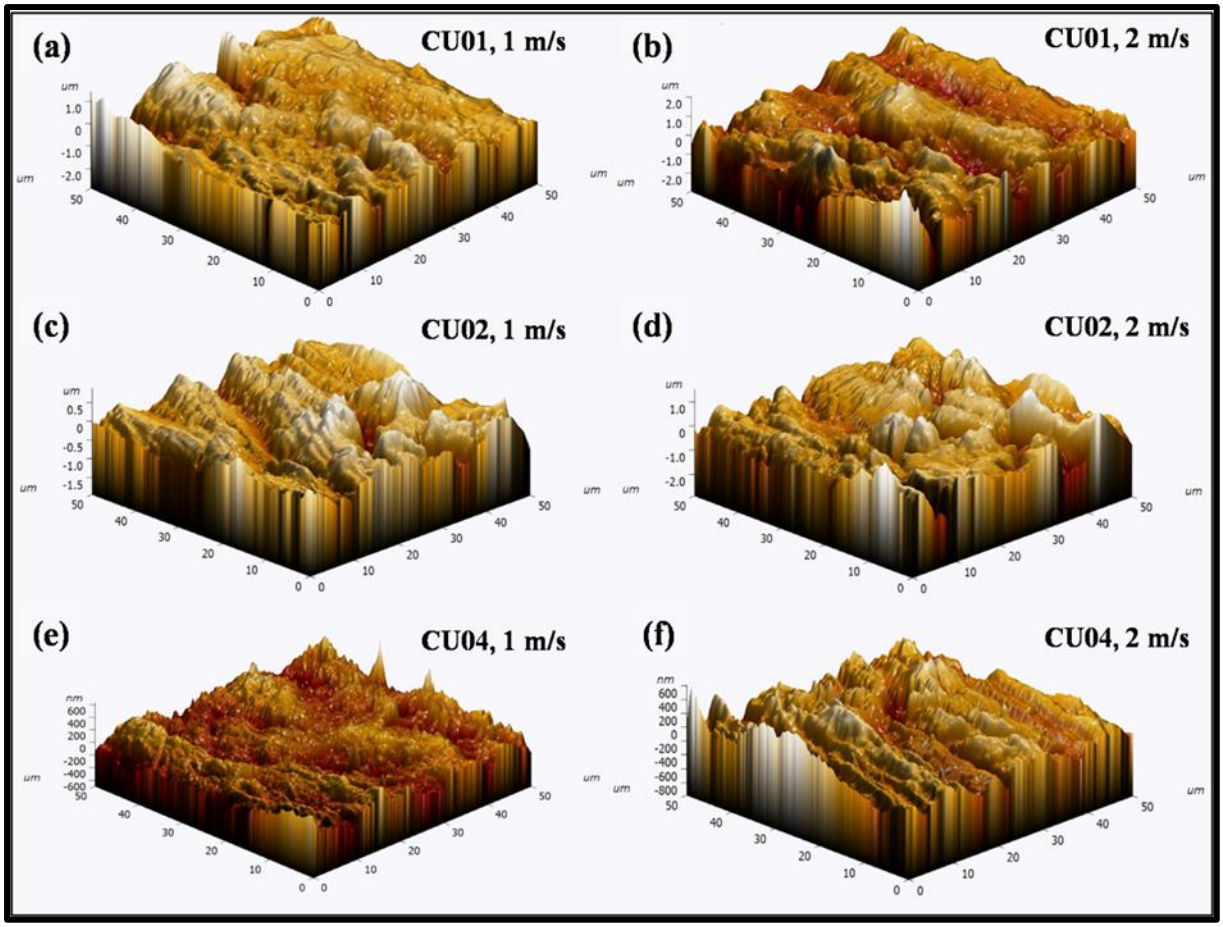

Figure 4.14. Atomic force microscopy (AFM) 3D morphology of the worn surfaces at an applied normal load of 30 N for a sliding distance of 2 km

Table 4.2. Surface roughness parameters of before and after wear of the developed materials at an applied normal load of 30 N for a sliding distance of 2 km.

Before Wear			
Parameters	**CU01**	**CU02**	**CU04**
Average roughness Ra (μm)	0.116	0.076	0.0421
Root mean square roughness Rq (μm)	0.229	0.117	0.0587

After Wear						
Parameters	**CU01 (1m/s)**	**CU01 (2m/s)**	**CU02 (1m/s)**	**CU02 (2m/s)**	**CU04 (1m/s)**	**CU04 (2m/s)**
Average roughness Ra (μm)	0.237	0.376	0.127	0.247	0.0610	0.0878
Root mean square roughness Rq (μm)	0.348	0.489	0.176	0.298	0.0810	0.1160

4.3 Conclusion

Copper composites such as CU02, CU03, and CU04 and unreinforced copper CU01 are successfully developed using the powder metallurgy technique, and its experimental analysis is performed for mechanical, physical, and tribological properties. The microstructural observations confirm the uniform distribution of reinforcing particles in the copper matrix during the sintering process. The primary conclusion of this work can be summarised as follows:

1) The XRD analysis of the developed composites confirms that there is no reaction between the copper matrix and reinforcement particles. It has also been discovered that XRD peak intensities increase with an increase in reinforcement content.
2) SEM examination of composites shows the homogeneous and uniform existence of reinforcement particles within the matrix. Some agglomeration is observed at increased reinforcement content. EDS elemental color mapping also reveals the presence of all the reinforcements in the copper matrix.
3) When the wt.% of boron carbide(B_4C) and graphite (Gr) in the copper matrix increases, the density of the composites decreases due to the reinforcement of a lower density of boron carbide(B_4C) and graphite (Gr) as compared to copper. Increasing the content of reinforcement increases the porosity of the composite as well.
4) The hardness of the developed composites improved significantly as compared to their matrix with the addition of boron carbide(B_4C) and graphite (Gr). Hardness increases significantly up to 3 wt.% B_4C + 3 wt.% Gr reinforcement in copper matrix and then decreases but is higher than the matrix. The maximum hardness observed in CU03 is 98.7 HV, which is a 69% improvement over pure copper (58.3 HV).

5) It is also observed that composites' wear rate and COF decrease as the reinforcing percentage increases. The lowest wear rate is seen in CU04, and this is due to the lubricating action of graphite (Gr) and harder boron carbide(B_4C) particles.
6) Analysis of the worn surfaces reveals that adhesion or delamination is the primary wear mechanism for pure copper specimens. However, boron carbide(B_4C) and graphite (Gr) reinforced composites depicted the abrasive, oxidative, and delamination modes of wear.